# Absolute Radiometric In-Flight Validation of Mid Infrared and Thermal Infrared Data From ASTER and MODIS on the Terra Spacecraft Using the Lake Tahoe, CA/NV, USA, Automated Validation Site

Simon J. Hook, R. Greg Vaughan, Hideyuki Tonooka, *Member, IEEE*, and S. Geoffrey Schladow

***Abstract*—In December 1999, the first Moderate Resolution Imaging Spectroradiometer (MODIS) instrument and an Advanced Spaceborne Thermal Emission and Reflection Radiometer (ASTER) instrument were launched into polar orbit on the Terra spacecraft. Both instruments measure surface radiance, which requires that they are calibrated and validated in flight. In-flight validation is essential to independently verify that instrument calibration correctly compensates for any changes in instrument response over time. In order to meet this requirement, an automated validation site was established at Lake Tahoe on the California/Nevada border in 1999 to validate the ASTER and MODIS thermal infrared (TIR, 7–13 $\mu$m) and MODIS mid infrared (MIR, 3–5 $\mu$m) land-monitoring channels. Daytime and nighttime data were used to validate the TIR channels, and only nighttime data were used to validate the MIR channels to avoid any reflected solar contribution. Sixty-nine ASTER scenes and 155 MODIS-Terra scenes acquired between years 2000 and 2005 with near-nadir views were validated. The percent differences between the predicted and instrument at-sensor radiances for ASTER channels 10–14 were $0.165 \pm 0.776$, $0.103 \pm 0.613$, $-0.305 \pm 0.613$, $-0.252 \pm 0.464$, and $-0.118 \pm 0.489$, respectively. The percent differences for MODIS-Terra channels 20, 22, 23, 29, 31, and 32 were $-1.375 \pm 0.973$, $-1.743 \pm 1.027$, $-0.898 \pm 0.970$, $0.082 \pm 0.631$, $0.044 \pm 0.541$, and $0.151 \pm 0.563$, respectively. The results indicate that the TIR at-sensor radiances from ASTER and MODIS-Terra have met the preflight radiometric calibration accuracy specification and provide well-calibrated data sets that are suitable for measuring absolute change. The results also show that the at-sensor radiances from the MODIS-Terra MIR channels have greater bias than expected based on the preflight radiometric calibration accuracy specification.**

Manuscript received May 2, 2006; revised September 14, 2006. The research described in this paper was carried out in part at the Jet Propulsion Laboratory, California Institute of Technology, under a contract with the National Aeronautics and Space Administration. Reference herein to any specific commercial product, process, or service by trade names, trademark, and manufacturer or otherwise does not imply endorsement by the United States or the Jet Propulsion Laboratory, California Institute of Technology.

S. J. Hook and R. G. Vaughan are with the NASA Jet Propulsion Laboratory, California Institute of Technology, Pasadena, CA 91109 USA.

H. Tonooka is with the Center for Information Technology, Ibaraki University, Ibaraki 316-8511, Japan.

S. G. Schladow is with the Department of Civil and Environmental Engineering and the Tahoe Environmental Research Center, University of California, Davis, CA 95616 USA.

Color versions of one or more of the figures in this paper are available online at http://ieeexplore.ieee.org.

Digital Object Identifier 10.1109/TGRS.2007.894564

***Index Terms*—Advanced Spaceborne Thermal Emission and Reflection Radiometer (ASTER), infrared, Moderate Resolution Imaging Spectroradiometer (MODIS), Tahoe, thermal, validation.**

## I. Introduction

IN-FLIGHT validation of mid infrared (MIR, 3–5 $\mu$m) and thermal infrared (TIR, 7–14 $\mu$m) data acquired by satellites and aircraft has long been recognized as an essential method to ensure their accuracy and precision. Several authors have conducted experiments to determine the in-flight spectral and radiometric calibration of MIR and TIR scanners mounted on aircraft and spacecraft (e.g., [2], [6]–[10], [13], [15], [18], [19], [23], and [24]).

These experiments typically involve measuring the radiance emitted by the surface at MIR and TIR wavelengths, and certain properties of the overlying atmosphere, and then inputting these data into a radiative transfer model to predict the at-sensor radiance. The predicted at-sensor radiance is then compared to the at-sensor radiance measured by the satellite or aircraft instrument. This approach is commonly referred to as the ground-based radiance method and is used in this paper. An alternate approach is to acquire data simultaneously with the satellite overpass from a well-characterized MIR and/or TIR sensor mounted on an aircraft and then propagate the aircraft radiance through a radiative transfer model to predict the radiance at the satellite. This approach is referred to as the aircraft radiance method. Both of these methods are loosely referred to as vicarious calibration.

The primary advantage of the airborne method is that little additional modification of the aircraft radiance to satellite altitudes is required because one of the primary contributors to the at-sensor radiance is atmospheric water vapor, most of which is typically beneath the aircraft. The primary disadvantage is that the calibration of the aircraft instrument may not be sufficiently well known.

The Lake Tahoe, California/Nevada (CA/NV), automated validation site was established in 1999 to help validate the MIR and TIR data and products from the Advanced Spaceborne Thermal Emission and Reflection Radiometer (ASTER) and Moderate Resolution Imaging Spectroradiometer (MODIS)

instruments. Large bodies of water are commonly used for validation because water is homogeneous and its emissivity is well known. Lake Tahoe, in particular, is ideally suited for radiometric validation for several additional reasons: 1) The lake does not freeze in the winter and is available year-round for validation. 2) The lake is large and can be used to validate sensors with pixel sizes ranging from meters to several kilometers. 3) The lake water is very pure; therefore, instruments are less susceptible to damage from salt and other substances typically found in water. 4) The University of California Davis, Tahoe Environmental Research Center (UCD) has a research station at the lake with two permanent research vessels, i.e., the R/V John LeConte and R/V Ted Franz, which provide excellent logistical support. 5) The lake is at 2-km elevation, and the total column water vapor is generally low (between 0.5- and 1.5-cm total column). Total column water vapor affects the forward propagation of surface radiance to the at-sensor radiance, and it is strongly desirable to have low total column water values, so any errors in the amount of water vapor have minimal impact on the forward calculation. 6) The lake has a wide range of surface skin temperature, from ∼278.15–298.15 K (5 °C–25 °C), allowing validation over a broad range of radiances. 7) Lake Tahoe is close to the three National Aeronautics and Space Administration (NASA) centers, including the Dryden Research Facility, which is used as a base for several NASA aircraft, therefore minimizing the cost of validating NASA MIR and TIR airborne sensors.

The ground-based radiance method is typically used for validating data acquired over the Lake Tahoe site; however, the site is also regularly overflown with airborne sensors, which are typically coincident with a satellite overpass, allowing both the ground- and airborne-radiance methods to be used simultaneously. The site is also being used to validate data from other sensors including the Along-Track Scanning Radiometer-2 [7], Landsat Enhanced Thematic Mapper Plus [2], Landsat-5 [8], and the Multispectral Thermal Imager [9].

## II. Instrument Summaries

The ASTER instrument was launched in 1999 on the first Earth Observing System platform (Terra). ASTER acquires data in 14 spectral channels in three instrument subsystems. The ASTER instrument does not acquire data in the MIR region. Channels 10–14, which make up the TIR subsystem and acquire data between 8.15 and 11.65 $\mu$m are the focus of this paper. The TIR subsystem incorporates a whiskbroom scanner that can be pointed $\pm 8.55^{\circ}$, allowing any spot on the Earth's surface to be imaged every 16 days. The TIR data are quantized in 12 bits, have a spatial resolution of ∼90 m at nadir, and are calibrated with a full-aperture honeycombed blackbody that can be heated from 270 to 340 K. The blackbody is viewed before and after each data acquisition and periodically heated to obtain calibration data at different temperatures. Most spaceborne TIR systems use blackbody values in conjunction with a view of deep space to perform two-point calibration. However, the ASTER TIR subsystem cannot view deep space, so these data are obtained by measuring the blackbody (set at 270 K) prior to each acquisition and then periodically heating and viewing the blackbody at four set-point temperatures (270, 300, 320, and 340 K). The imaging of the blackbody prior to each Earth observation is referred to as short-term calibration, and the periodic imaging of the blackbody at a series of set-point temperatures is referred to as long-term calibration (LTC). In the early part of the mission, LTCs were executed every 17 days; then, in April 2001, this interval was increased to 33 days in order to satisfy a requirement to minimize the number of pointings of the shortwave-infrared subsystem. The preflight radiometric calibration accuracy requirement for ASTER channels 10–14 is $< 1$ K for temperatures between 270 and 340 K [20]. More details on the calibration approach are given in [11], [19], and [20].

The first MODIS instrument was also included on the Terra platform. MODIS acquires data in 36 spectral channels. Channels 20, 22, 23, 29, 31, and 32 are the focus of this paper. However, channels 21, 24, and 25, which are between 3 and 5 $\mu$m, and channels 28, 30, and 33, which are between 7 and 14 $\mu$m, can also be partially validated with the field measurements. Absolute validation of channels 21, 24, 25, 28, 30, and 33 is limited because they are strongly affected by the atmosphere (some are atmospheric sounding channels); therefore, the forward calculation of the surface values to the sensor is much more sensitive to the radiative transfer model and associated inputs. Nonetheless, useful validation data can be obtained from these channels, and validation results are available from the first author upon request. MODIS scans $\pm 55^{\circ}$ from nadir and provides daytime and nighttime imaging of any point on the Earth every 1–2 days with a continuous duty cycle. MODIS data are quantized in 12 bits and have a spatial resolution of ∼1 km at nadir. They are calibrated with a cold space view and full-aperture blackbody viewed before and after each Earth view. There are two MODIS instruments in space, i.e., one on the Terra platform and the second instrument on the Aqua platform. This paper only reports on the performance of the MODIS instrument on the Terra platform. The preflight radiometric calibration accuracy requirement for MODIS channels 20, 22, 23, 29, 31, and 32 are 0.75%, 1.0%, 1.0%, 1.0%, 0.5%, and 0.5%, respectively [5]. A more detailed description of the MODIS instrument and its potential application is given in [1] and [16].

This paper reports on the results of using the ground-based radiance method to validate the absolute radiometric calibration of ASTER channels 10 (8.29 $\mu$m), 11 (8.63 $\mu$m), 12 (9.08 $\mu$m), 13 (10.66 $\mu$m), and 14 (11.29 $\mu$m), and MODIS-Terra channels 20 (3.79 $\mu$m), 22 (3.97 $\mu$m), 23 (4.06 $\mu$m), 29 (8.53 $\mu$m), 31 (11.01 $\mu$m), and 32 (12.03 $\mu$m). The values given in brackets are the centroid wavelength value. Note that the centroid value accounts for any differences in the system response function from a Gaussian response and can be different from the center wavelength for a given channel.

## III. Physical Framework

The at-sensor radiance $Ls$ for a given wavelength $\lambda$ in MIR and TIR, excluding any solar contribution in the MIR, can be written as

$$Ls_{\lambda} = \left[\varepsilon_{\lambda} L_{\mathrm{bb}\lambda}(T) + (1-\varepsilon_{\lambda}) L_{\mathrm{sky}\lambda}\right] \tau_{\lambda} + L_{\mathrm{atm}\lambda} \quad (1)$$

where

- $\varepsilon_\lambda$ surface spectral emissivity at a given wavelength ($\lambda$);
- $L_{\mathrm{bb}\lambda}(T)$ spectral radiance from a blackbody at surface temperature $T$;
- $L_{\mathrm{sky}\lambda}$ sky radiance (spectral downwelling radiance incident upon the surface from the atmosphere);
- $\tau_\lambda$ spectral atmospheric transmission (transmittance);
- $L_{\mathrm{atm}\lambda}$ path radiance (spectral upwelling radiance from atmospheric emission and scattering that reaches the sensor).

The effect of $\tau_\lambda$ is to reduce the amount of ground-emitted radiance measured at the sensor; $L_{\mathrm{atm}\lambda}$ adds a component unrelated to the ground, and $L_{\mathrm{sky}\lambda}$ serves to reduce the spectral contrast since the deeper an emissivity feature, the more it is "filled in" by reflected downwelling radiation due to Kirchhoffs's law. Once the atmospheric effects have been removed, the surface radiance is given by

$$L_\lambda = \varepsilon_\lambda L_{\mathrm{BB}\lambda}(T)$$

$$L_{\mathrm{BB}\lambda} = \frac{C_1}{\lambda^5 \pi \left[e^{\left(\frac{C_2}{\lambda T}\right)} - 1\right]} \tag{2}$$

where

- $L_\lambda$ emitted radiance (in $\mathrm{W} \cdot \mathrm{m}^{-2} \cdot (\mathrm{m} - \Delta\lambda)^{-1} \cdot \mathrm{sr}^{-1}$);
- $L_{\mathrm{BB}\lambda}$ blackbody radiance (in $\mathrm{W} \cdot \mathrm{m}^{-2} \cdot (\mathrm{m} - \Delta\lambda)^{-1} \cdot \mathrm{sr}^{-1}$);
- $\lambda$ wavelength of channel (in meters);
- $T$ temperature of blackbody (in degrees Kelvin);
- $C_1$ first radiation constant, $3.7415 \times 10^{-16}$ W $\cdot$ m$^2$;
- $C_2$ second radiation constant, $0.0143879$ m $\cdot$ K;
- $\varepsilon_\lambda$ surface spectral emissivity at a given wavelength $\lambda$.

Surface temperature $T$ is not an intrinsic property of the surface; it varies with external factors such as irradiance history and meteorological conditions. Conversely, emissivity is a characteristic of the material making up the surface and is independent of the temperature. For most terrestrial surfaces, $200\ \mathrm{K} < T < 340\ \mathrm{K}$, although a more restricted range of ~270–310 K brackets most of the temperatures outside the polar regions and deserts for typical conditions. The emissivities for the most natural surfaces in the wavelength range covered by the MODIS and ASTER TIR channels typically range from ~0.7 to 1 [12], although surfaces with emissivities $< 0.85$ are largely restricted to arid and semiarid regions.

Equation (2) describes the radiance from a homogeneous isothermal surface. However, many surfaces at the resolution of ASTER or MODIS will consist of several materials at different temperatures and emissivities. Insufficient information to deal with surfaces comprising multiple materials with different temperatures and emissivities is present in the spaceborne data; thus, validation sites where these effects are minimized, such as water, are typically used. It should be noted that, since each ASTER or MODIS channel spans a wavelength range, the radiance for a given channel is integrated over that range. Since the ASTER or MODIS channels are fairly narrow, any uncertainty introduced by this irreversible operation is small.

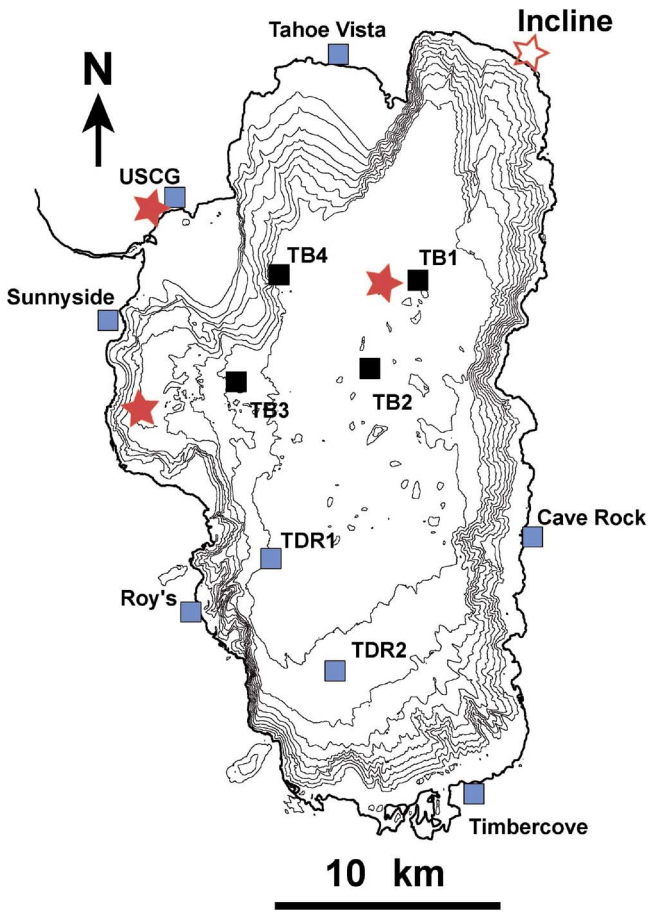


Fig. 1. Bathymetric map of Lake Tahoe, CA/NV, with a contour interval of 50 m. The four NASA buoys are labeled TB1, TB2, TB3, and TB4. Also shown are the USCG station and other meteorological stations around the lake. Water properties are measured at the Midlake (star near TB1) and the Index station (star south of Sunnyside). Meteorological measurements have been made at both the Incline (open star) and the USCG (closed star). UCD also maintains two additional floats (rafts) in the southern part of Lake Tahoe (TDR1 and TDR2), which measure meteorological variables and bulk temperature.

## IV. Site Location and Characteristics

Lake Tahoe is a large lake situated in a granite graben near the crest of the Sierra Nevada Mountains on the CA/NV border, at 39° N, 120° W. The lake level is approximately 1895 m above mean sea level. The lake is roughly oval in shape with a north–south major axis (33 km long and 18 km wide) and has a surface area of 500 km$^2$ (Fig. 1). The land portion of the watershed has an area of 800 km$^2$. Lake Tahoe is the 11th deepest lake in the world, with an average depth of 330 m, a maximum depth of 501 m, and a total volume of 156 km$^3$. The surface layer of Lake Tahoe deepens during the fall and winter. Complete vertical mixing only occurs every few years [17]. Due to its large thermal mass, Lake Tahoe does not freeze in winter. There are approximately 63 streams/rivers flowing into Lake Tahoe and only one river flowing out, i.e., the Truckee River.

## V. Site Infrastructure and Field Measurement

Measurements at the site are made from four permanently moored buoys on the lake referred to as TB1, TB2, TB3,

and TB4 and the U.S. Coast Guard (USCG) station located on the northwest shore of the lake (Fig. 1). Each buoy has a custom-built radiometer that measures skin temperature and several temperature sensors that measure the bulk water temperature at multiple depths (∼2–15 cm, 0.5 m, 1.0 m, 1.5 m, and 5.5 m). The radiometers were built at the Jet Propulsion Laboratory (JPL), and two radiometer models have been deployed at the site. The earlier model had an accuracy of ±0.2 K, and the later model has an accuracy of ±0.1 K. The radiometers are calibrated in the laboratory using a National Institute for Standards and Technology (NIST)-traceable stirred-water-bath blackbody [9]. The accuracy of the JPL radiometers was independently verified in both the laboratory and in a field comparison [3], [14]. The results indicate that the JPL radiometers agree with other well-calibrated radiometers to within ±0.05 K [3]. The temperature sensors are recalibrated at JPL using a temperature-controlled water bath with a NIST-traceable thermometer before and after deployments. Details of the sensor types and JPL calibration facility are provided in [9]. During the monitoring period, meteorological stations were added to each buoy. The meteorological measurements include wind speed, wind direction, relative humidity, air temperature, atmospheric pressure and net radiation. A full set of measurements (meteorology, bulk, and skin temperatures) are made every 2–5 min and stored on data loggers, which are read out either daily via telephone modem or every few months during site visits.

Both NASA/JPL and UCD maintain additional equipment at the USCG station. This includes a full meteorological station (wind speed, wind direction, relative humidity, air temperature, and atmospheric pressure), a full radiation station (long- and short-wave radiation up and down), a shadow-band radiometer, and an all-sky camera. The shadow-band radiometer provides information on total water vapor and aerosol optical depth. The latitude and longitude of the four NASA buoys are given in [9] and at http://calval.jpl.nasa.gov.

Atmospheric profiles for the site are obtained from model data generated by the National Center for Environmental Prediction (NCEP). NCEP produces global model values on a $1^\circ \times 1^\circ$ grid at 6-h intervals. Lake Tahoe is on a grid point, and the NCEP data are interpolated to the overpass time.

Additional measurements including primary productivity, nutrient concentration (various forms of nitrogen and phosphorus), chlorophyll concentration, light penetration, temperature distribution, and secchi-disk transparency are made from the UCD Research Vessel John LeConte at approximately 10-day intervals. A more detailed description of the site is given in [7], [9].

## VI. Data Reduction and Validation Methodology

In order to validate the at-sensor radiance measured by a satellite sensor, it is necessary to derive and compare the equivalent at-sensor radiance from the field measurements. The following steps summarize the procedure for undertaking such a comparison.

- Extract the bulk temperature.
- Extract the radiometric temperature.
- Correct the radiometric temperature to skin kinetic temperature.
- Propagate the skin temperature to the satellite using a radiative transfer model (MODTRAN 3.5) and interpolated atmospheric profile.
- Convolve the propagated at-sensor radiance to the instrument response function to obtain the vicarious radiance (VR).
- Extract the image radiance derived with the onboard calibrator (OBC) (ASTER product AST01B and MODIS product MOD02).
- Compare and contrast the OBC and VR values.

Initially, the bulk water temperature was extracted from the temperature sensors that were placed ∼2–15 cm beneath the surface on the float tethered behind each buoy at the time of the Terra overpasses. The bulk water temperature was calculated as the mean of the measured temperatures at the time of the overpass. Each buoy typically has four temperature sensors attached to the float but may have as many as 12 sensors at a depth ranging from 2 to 15 cm. Since the temperature sensors "ride" on a float attached to the buoy, the exact depth varies, depending on the state of water surface. Prior to inclusion in the mean, the temperature trace of each sensor was examined and cross compared with the other sensors on the same buoy to check if all sensors were reading correctly. The standard deviation of the sensors was also calculated and was typically about 0.1 K (see Section VIII).

In order to compare the radiometer measurements to the satellite radiometric measurements, it is necessary to correct the field measurements to surface kinetic or skin temperatures, so they can be propagated through the atmosphere using the radiative transfer code (RTC) (MODTRAN 3.5, [4]). Once propagated, the atmospheric radiance is convolved to the instrument system response functions and compared with the instrument at-sensor radiances. The surface skin temperature is required since the field radiometers measure the radiometric temperature over a broader wavelength range than the satellite radiometers. In order to obtain the surface skin temperature, the radiometer data must be corrected for the reflected downwelling radiation from the atmosphere and the nonunit emissivity of the water. Correction for the downwelling sky radiance reflected by the surface into the path of the radiometer involves using a radiative transfer model driven by an atmospheric profile to estimate the downwelling sky radiation contribution and is described in [7] and [8]. The atmospheric profile was obtained from NCEP data interpolated to the overpass time, as described in the site infrastructure and measurements section. The emissivity of the water was obtained from the ASTER spectral library available at http://speclib.jpl.nasa.gov.

In some cases, the skin temperature was not available at *any* buoy for a given overpass or for a particular buoy on a given overpass due to equipment failure. If no skin (radiometer) temperatures were available for *any* buoys for a given overpass, the average skin effect (bulk minus skin temperature) for *all* overpasses was subtracted from the average bulk temperature (with a depth of 2–15 cm) at each buoy to obtain the buoy skin temperature. If skin temperatures were available at some but not all buoys for a given overpass, then the average skin effect

(bulk minus skin temperature) for *that* overpass was calculated and subtracted from the bulk temperatures (with a depth of 2–15 cm) to obtain the skin temperatures for the buoys without a working radiometer. These two approaches were used to maximize the number of validation opportunities. The bulk and skin temperatures are available from the lead author upon request.

The skin temperature was found to be, on average, $0.22 \pm 0.61$ K cooler than the bulk temperature during the day and $0.39 \pm 0.27$ K cooler than the bulk temperature at night. The Terra daytime overpasses were between 18:50 (GMT) and 19:13 (GMT), and the nighttime overpasses were between 6:00 (GMT) and 6:22 (GMT). GMT can be converted to local (Pacific) time by subtracting 8 h. The smaller skin effect and greater scatter in the skin effect during the day were attributed to solar heating.

The skin temperatures were then propagated to at-sensor radiance using the same RTC and atmospheric profile used to correct the radiometric data to skin temperature, and the at-sensor radiance was convolved with the instrument system response functions to obtain an equivalent predicted or vicarious instrument at-sensor radiance.

## VII. Error Analysis of Procedure for Validation of In-Flight Radiometric Calibration

There are four primary sources of error in deriving the at-sensor radiance from the field data at the water site. They are given as follows:

- radiometer accuracy, precision, and uncertainty;
- correction for downwelling sky radiance in the radiometer data to obtain the surface kinetic temperature;
- atmospheric profile errors due to incorrect representation of the atmosphere in the profile used in the radiative transfer model to propagate the surface kinetic temperature to the at-sensor radiance;
- site heterogeneity.

The preceding list assumes that the emissivity of the surface is known and constant, which is true for a water surface when the measurements are made with a radiometer with near-nadir viewing, as is the case with the Lake Tahoe measurements. If the radiance from the water surface is measured at off-nadir angles or at varying wind speeds, the emissivity does vary and can be determined using an emissivity model, e.g., [25].

### A. Radiometer Accuracy, Precision, and Uncertainty

The accuracy, precision, and uncertainty values for a typical JPL radiometer are 0.08, 0.03, and 0.085 K, respectively. These values are determined by first calibrating the radiometer over the temperature range of 277.15–333.15 K (4 °C–60 °C) and then using the calibrated radiometer to measure the temperature of a blackbody over that same range.

### B. Correction for Downwelling Sky Radiance

The JPL radiometer does not make a measurement of the sky temperature; therefore, the contribution to the radiometer signal from the downwelling sky radiance is calculated using an RTC and removed. The need to correct the radiometric temperature measured by the radiometers to skin temperature with downwelling radiance derived from the NCEP data introduces an uncertainty in the skin temperature. This uncertainty is very small ($< 0.01$ K) and is discussed more fully in [7].

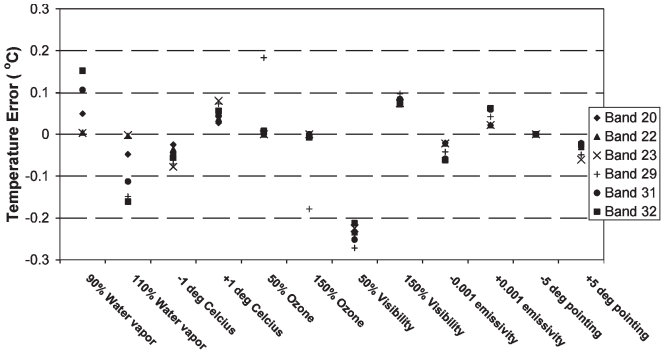


Fig. 2. Plot of the brightness temperature error associated with perturbing the atmospheric profile, varying the path length (pointing error), and assuming an incorrect emissivity for the MODIS channels. The temperature error for profile perturbations was obtained by calculating nominal radiance with a U.S. standard atmosphere at Lake Tahoe elevations and with the emissivity of water, modifying the input profile, recalculating the radiance, and then calculating the at-sensor temperature difference between the nominal and adjusted profiles.

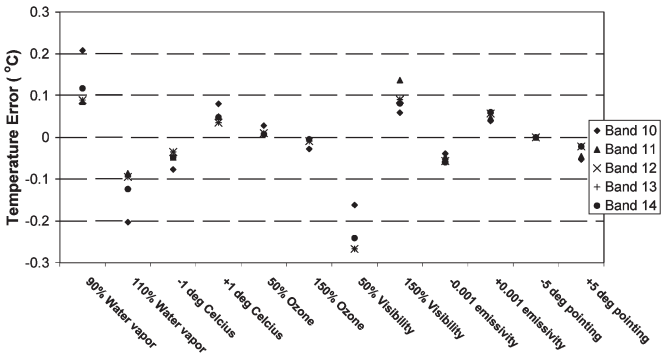


Fig. 3. Plot of the brightness temperature error associated with perturbing the atmospheric profile, varying the path length (pointing error), and assuming an incorrect emissivity for the ASTER channels. The temperature error for profile perturbations was obtained by calculating nominal radiance with a U.S. standard atmosphere at Lake Tahoe elevations and with the emissivity of water, modifying the input profile, recalculating the radiance, and then calculating the at-sensor temperature difference between the nominal and adjusted profiles.

### C. Atmospheric Profile Errors

Any error in the atmospheric profile when it is used to propagate the ground radiance (calculated from the kinetic temperature derived from the radiometer and assumed emissivity for water) to the altitude of the satellite sensor will result in an error in the predicted at-sensor radiance. This error will vary depending on the wavelength range covered by the channel that is being studied. In order to assess this error, various profile inputs were modified, and the difference between using the actual profile and the modified profile was calculated; these results are summarized in Figs. 2 and 3 for MODIS and ASTER, respectively. This forward calculation assumes that one has the skin temperature; if one is forward calculating the bulk temperature, then there will be an additional error associated with the skin effect. These figures also show the effect of an emissivity error and pointing error.

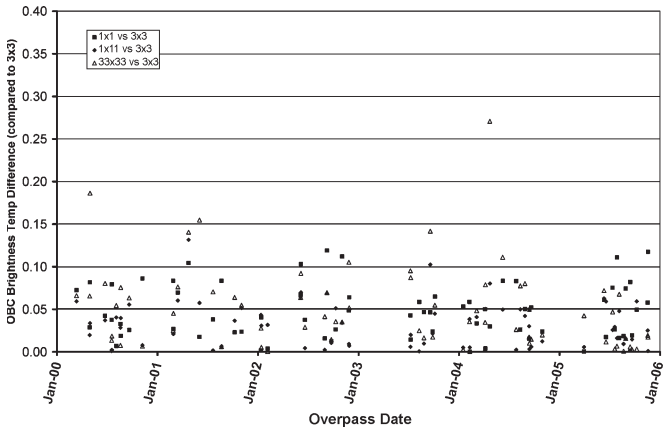


Fig. 4. Plot of the difference between the average brightness temperature for $3 \times 3$ pixel areas centered on each buoy and differently sized areas for the ASTER validation overpasses at Lake Tahoe. The average difference for a given sized area on a given day was obtained by averaging the differences of the desired area size centered on each buoy with the $3 \times 3$ average.

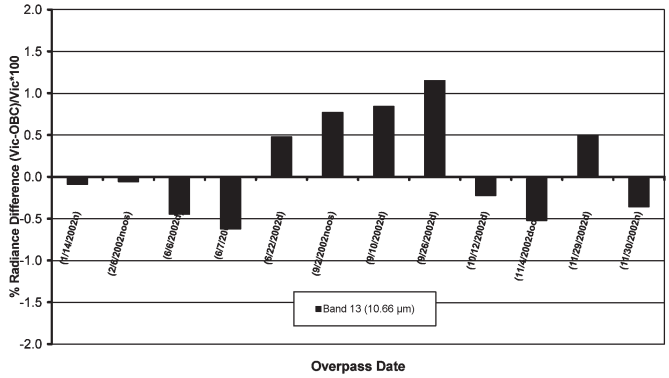


Fig. 5. Plot of the average percent difference between the vicarious (V) and ASTER OBC derived radiances for ASTER TIR channel 13 at the Terra overpass times from January to November 2002. Percent difference is calculated as $(\text{V-OBC})/\text{V} \times 100$. The average percent difference is the average percent difference for all buoys operating during overpass (maximum of four buoys).

Examination of Fig. 2 indicates that the MODIS MIR channels (20, 22, and 23) are least affected by various errors with values that are typically less than 0.05 K. The largest errors are associated with a reduction in visibility or change in the total column water vapor. The U.S. Standard Atmosphere profile was used in the error assessment and contains more water vapor than is typical at Lake Tahoe (total column water of 0.5–1.5 cm), but because of the altitude of the site, the effect is small for most of the channels that are located in the "clear" regions of the atmosphere. For example, a 10% error in the water vapor profile results in an error in the at-sensor brightness temperature of $\sim$0.1 K for MODIS channel 31 (Fig. 2). The size of this error would be greater for a wetter warmer atmosphere at sea level. It should be noted that the MODTRAN RTC also adds some error related to the band models it uses. These errors are discussed in detail in [21] and [22].

### *D. Site Heterogeneity*

As part of the validation procedure, the instrument at-sensor radiance is compared with the predicted at-sensor radiance. The instrument at-sensor radiance is calculated as the average of $3 \times 3$ pixels centered on the nominal buoy location. A $3 \times 3$ pixel area is used to avoid problems with any particular detector and also provide a sampling of all the detectors while avoiding any land contamination. Both ASTER and MODIS have ten detectors in each channel. In the case of ASTER, this corresponds to a $270 \times 270$ m$^2$ area, and in the case of MODIS, this corresponds to a $3 \times 3$ km$^2$ area. In order to assess site homogeneity, which varies with both time and location on the lake, the average difference of the value for a $3 \times 3$ area centered on each buoy in the ASTER data and several other sized areas centered on each buoy was calculated (Fig. 4). The other sized areas were $1 \times 1$, $11 \times 11$, and $33 \times 33$ ASTER pixels corresponding to $90 \times 90$ m$^2$, $1 \times 1$ km$^2$, and $3 \times 3$ km$^2$, respectively. These sizes were picked to provide an indication of how much of the difference between an ASTER and MODIS validation could be due to differences in homogeneity. If the temperature of the lake was perfectly homogeneous, there should be no difference in temperature between the $3 \times 3$ pixel area and the other sized areas.

Examination of Fig. 4 indicates that this difference is below 0.16 K for all but two dates, indicating that the lake is generally homogeneous at a variety of scales. There are a couple of dates (April 30, 2000 and April 25, 2004) that have larger differences of 0.19 and 0.27 K, respectively. These dates both occur in April, when the lake shows more heterogeneity as it begins to warm rapidly from its wintertime minimum of $\sim$278.15 K (5 °C). The heterogeneity is the result of upwellings and increased mixing. Upwellings typically occur after strong wind events, when the wind forces the warmer surface waters to the downwind side of the lake, causing colder deeper water to upwell on the upwind side of the lake (see [17] for further details). Although these April data indicate that the surface was more heterogeneous than normal, the validations were still within the typical range and were included in the results. This analysis does not assess site homogeneity at scales less than the 90-m size of the ASTER pixel. Higher spatial resolution data would be required to evaluate variability within the 90-m pixel. No attempt was made to see if the buoy itself influenced the temperature of the water that was being measured. It was assumed that the water measured by the bulk temperature sensors and radiometers was always moving past the buoy due to current motion.

## VIII. Result and Discussion

### *A. ASTER Results*

Fig. 5 shows the percent difference of the predicted and measured radiances for the ASTER channel that was least affected by the atmosphere (channel 13) for the period from January 14, 2002, to November 2002. Examination of this plot indicates that the difference between the predicted and measured values was at the level of a few tenths of a percent; then starting around June 22, 2002, the difference increased until September 26, 2002, when it returned to slightly negative values. On September 26, 2002, the difference is greater than the 1% level, a change which is equivalent to 0.65 K and at the calibration requirement limit at this wavelength. This increase in radiance

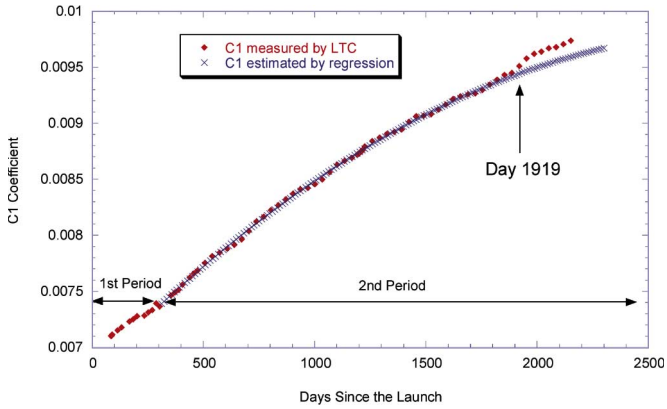


Fig. 6. Change in the C1 response (gain) for an ASTER channel since launch. Data have been separated into three different epochs based on change in response.

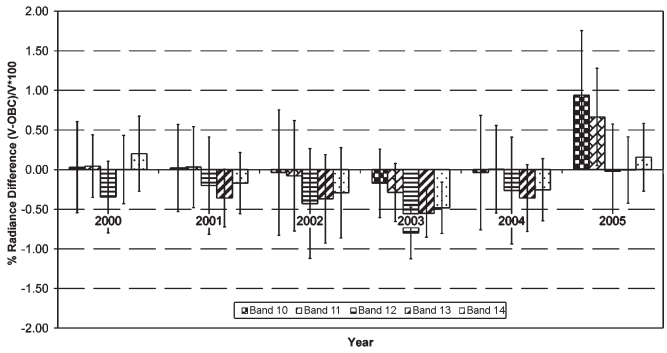


Fig. 7. Plot of the average percent difference and standard deviation between the vicarious (V) and ASTER OBC-derived radiances for all validated overpasses for a given year from 2000 to 2005. Percent difference is calculated as $(\text{V-OBC})/\text{V} \times 100$. On a given overpass, there are up to four matchups (one per buoy); the average of these differences is calculated, and this average value is used in the calculation of the average annual value. The standard deviation is also calculated from the average differences for each overpass.

error, followed by a sharp correction, is due to the instrument response degrading with time and being periodically corrected with updated coefficients derived from the onboard blackbody from the LTCs. The LTCs are undertaken frequently, but the data from the LTCs were only used to develop and implement a new set of calibration coefficients if the change between the last calibration coefficient update and the latest LTC was greater than a certain threshold. Even when this threshold was passed, updated coefficients were not rapidly implemented, causing the threshold to be passed before the new coefficients were in place. This situation was made worse by the rate of instrument degradation increasing over time and resulted in the appearance of a "sawtooth" pattern in the validation results.

In order to remedy this effect, the ASTER science team developed web-accessible software that allows the user to input the date of an image acquisition together with the calibration version and obtain the appropriate correction to apply to the image for the drift. More details of the software and the approach are given in [19]. In the future, this approach will be replaced by fitting a curve to all the LTC data. An example of the curve-fitting approach is illustrated in Fig. 6 for one detector from one channel. The advantage with this approach is that the change in response for each new acquisition is "predicted" by the curve-fit equation and that a separate curve can be applied to every detector as opposed to the current approach, which uses a single correction factor for all detectors. Each ASTER channel has ten detectors, and the LTC data indicate that, while all the detectors are degrading at similar rates, the degradation rates are not identical with a notable difference between the odd and even detectors. It is anticipated that multiple equations may be required to fit the curve covering different epochs. For example, in Fig. 6, a different curve-fit equation may be applied after day 1919 (January 3, 2005). The cause for the change after day 1919 has not been determined. It is planned that the ASTER calibration committee will convene during each ASTER team meeting twice per year to determine if a new equation is required.

Fig. 7 shows the percent difference between the predicted and measured radiances for ASTER channels 10–14 calculated for each year starting in 2000 after correction with the [19] method discussed previously. Sixty-nine ASTER scenes were validated at Lake Tahoe, which included 11, 9, 13, 7, 15, and 14 scenes acquired in 2000, 2001, 2002, 2003, 2004, and 2005, respectively. Of the 69 dates evaluated, radiometer data were available for 59 of them; for the other ten dates, bulk temperature data were used with an average skin effect calculated from the 59 dates with radiometer data. On each validation day, there were up to a maximum of four matchups (one per buoy) for a total of 246 independent validations for surface temperatures ranging between 278.15 and 296.15 K (5 °C and 23 °C). These results indicate that, after correction, any bias between the predicted and measured radiances for the ASTER thermal channels has remained within $\pm 1\%$ and was typically better than $\pm 0.5\%$, indicating that all channels are well within the preflight specification of $\pm 1$ K. Generally, the largest differences are observed in the channels that are most affected by the atmosphere (channels 10, 12, and 14), suggesting that errors in the forward calculation of the surface radiances through the atmosphere affect the validation of these channels. With the exception of the results from 2005, the majority of the differences are negative, i.e., the instrument radiances are higher than the predicted radiances. Prior to the sawtooth correction, these differences were positive since the instrument measured radiance was decreasing for a given energy input. These results suggest that the ASTER standard adjustment may be a slight overcorrection. Starting in 2005, the bias is very small for channels 12–14. However, channels 10 and 11 show a larger ($\sim 0.5\%$) positive difference. There are two dates that show unusually large biases in channels 10 and 11 in the 2005 data set, but even if these are removed, there remains a positive bias. Further data are required to determine if the positive bias observed in these channels will be the norm and also whether the new calibration scheme will have an impact on these channels.

### B. MODIS-Terra Results

Fig. 8 shows a plot of the percent radiance difference between the predicted (vicarious) at-sensor radiance and measured (OBC) radiance for MODIS-Terra channels 29, 31, and 32, starting in 2000. One hundred and fifty-five MODIS-Terra TIR scenes were validated at Lake Tahoe, which included 24, 23, 31, 16, 29, and 32 scenes acquired in 2000, 2001, 2002,

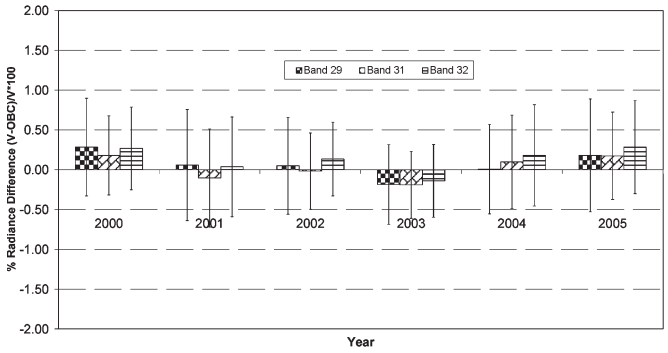


Fig. 8. Plot of the average percent difference and standard deviation between the vicarious (V) and MODIS-Terra TIR OBC-derived radiances for all validated overpasses for a given year from 2000 to 2005. Percent difference is calculated as $(\text{V-OBC})/\text{V} \times 100$. On a given overpass, there are up to four matchups (one per buoy); the average of these differences is calculated, and this average value is used in the calculation of the average annual value. The standard deviation is also calculated from the average differences for each overpass.

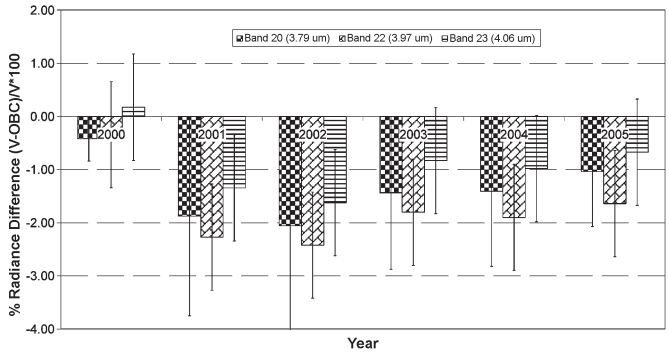


Fig. 9. Plot of the average percent difference and standard deviation between the vicarious (V) and MODIS-Terra MIR OBC-derived radiances for all validated overpasses for a given year from 2000 to 2005. Percent difference is calculated as $(\text{V-OBC})/\text{V} \times 100$. On a given overpass, there are up to four matchups (one per buoy); the average of these differences is calculated, and this average value is used in the calculation of the average annual value. The standard deviation is also calculated from the average differences for each overpass.

2003, 2004, and 2005, respectively. All results were obtained using MODIS-Terra version 4 data. On each validation day, there were typically four matchups (one per buoy) for a total of 582 independent validations. Of the 155 dates evaluated, radiometer data were available for 139 of them; for the other 16 dates, bulk temperature data were used with an average skin effect calculated from the 139 dates with radiometer data. The validations were undertaken approximately every 16 days, include a day and a night validation, and cover the range of 278.15–296.15 K (5 °C–23 °C). The 16-day cycle was centered on the nadir overpass. The original specification for the MODIS-Terra instrument required that the absolute radiometric calibration accuracy of the instrument be at the 0.5%–1.0% radiance level, depending on the channel. Fig. 8 clearly shows that the MODIS-Terra instrument has met that specification for channels 29, 31, and 32, which were used for land studies for the duration of the mission, thus far, with differences within $\pm 0.25\%$ ($\sim$0.16 K).

Fig. 9 shows a plot of the percent radiance difference between the predicted (vicarious) at-sensor radiance and measured (OBC) radiance for the MODIS-Terra MIR channels for each year starting in 2000. Seventy-eight MODIS-Terra MIR scenes (nighttime only) were validated at Lake Tahoe, which included 13, 13, 16, 7, 12, and 17 scenes acquired in 2000, 2001, 2002, 2003, 2004, and 2005, respectively. Starting in 2001, there was a noticeable negative bias in the MODIS-Terra MIR channels, which varies between $-0.5\%$ and $-2\%$ depending on the channel but has remained consistent for a given channel. The exact causes for this bias remain unresolved; however, in 2000 and 2001, various adjustments were made to the MODIS-Terra instrument, and it is possible that one of these adjustments resulted in a change to a bias in the range of $-0.5\%$ to $-2.0\%$, depending on the MIR channel. Preliminary validation results from MODIS-Aqua data indicate that the TIR data have similar accuracies to the MODIS-Terra data and that the MODIS-Aqua MIR data do not show the bias observed in the MODIS-Terra MIR data.

The results from both ASTER and MODIS-Terra are summarized in Table I for the entire validation period. On a given overpass, there are up to four matchups (one per buoy); the average of these differences is calculated, and this average value is used in the calculation of the overall average value. The standard deviation is also calculated from the average differences for each overpass. The standard deviation provides a measure of the amount of variability in the validation results and should be similar to the total error budget from the error analysis presented earlier, *provided* that the instrument is well calibrated. For example, the standard deviation of the validation result for channel 31 is 0.33 K, which is similar to the theoretical error described in the error analysis section (radiometer error, profile error, heterogeneity error, etc.). If the bias is greater than the theoretical error, it is likely that there is a problem with the instrument calibration. The results indicate that the instrument-calibrated radiances of the ASTER and MODIS-Terra TIR channels continue to meet or better the preflight specification, provided that the ASTER channels are corrected for the additional drift between LTCs. The need for periodic LTCs arises because ASTER uses a single blackbody and does not have a space view, unlike MODIS, which has both a blackbody and a space view. The additional complexity in the calibration that arises if a space view is not available should be considered in the design stages, and it should be recognized that further effort will be required once the instrument is in operation. The degradation of the ASTER TIR system was not expected nor was the difference in the rate of the degradation of the odd versus even ASTER detectors. In addition, the problems with the MODIS-Terra MIR data were not expected. The results demonstrate the need to independently validate the in-flight calibration of MIR and TIR data. The results demonstrate the need for continued validation of ASTER and MODIS-Terra MIR and TIR data as well comparison with other instruments such as MODIS-Aqua. If an instrument does not meet its calibration specification, it is likely that the downstream products, e.g., temperature and emissivity, will not also meet the specification. While every effort may be made to ensure good onboard calibration, it is still necessary to validate the calibration in-flight to correct any additional artifacts, which may not have been anticipated.

TABLE I
AVERAGE PERCENT DIFFERENCE AND STANDARD DEVIATION BETWEEN THE VICARIOUS (V) AND OBC-DERIVED RADIANCES FOR ALL VALIDATED OVERPASSES FOR A GIVEN CHANNEL FROM EITHER ASTER OR MODIS-TERRA FOR THE PERIOD FROM 2000 TO 2005. PERCENT DIFFERENCE IS CALCULATED AS (V-OBC)/V × 100. ON A GIVEN OVERPASS, THERE ARE UP TO FOUR MATCHUPS (ONE PER BUOY). THE AVERAGE OF THESE DIFFERENCES IS CALCULATED, AND THIS AVERAGE VALUE IS USED IN THE CALCULATION OF THE OVERALL AVERAGE VALUE. THE STANDARD DEVIATION IS ALSO CALCULATED FROM THE AVERAGE DIFFERENCES FOR EACH OVERPASS. THE PREFLIGHT CALIBRATION ACCURACY SPECIFICATION COLUMN SHOULD BE COMPARED WITH THE PERCENT RADIANCE DIFFERENCE COLUMN

| Sensor | Band and Center (μm) | Preflight Calibration Accuracy Spec. | Number of Dates Validated | Average of % Radiance Difference (BIAS) | Std Dev of % Radiance Difference | Range of % Radiance Difference (max-min) | Average of BT Difference (K) (BIAS) | Std. Dev of BT Difference (K) | Range of BT Difference (K) (max-min) |
|---|---|---|---|---|---|---|---|---|---|
| MODIS | 20 (3.79) | < 0.75% | 78 | -1.375 | 0.973 | 5.059 | | | |
| MODIS | 22 (3.97) | < 1.0% | (nighttime | -1.743 | 1.027 | 5.987 | | | |
| MODIS | 23 (4.06) | < 1.0% | only) | -0.898 | 0.970 | 5.764 | | | |
| MODIS | 29 (8.53) | < 1.0% | | 0.082 | 0.631 | 3.369 | 0.039 | 0.299 | 1.566 |
| MODIS | 31 (11.02) | < 0.5% | 155 | 0.044 | 0.541 | 3.086 | 0.024 | 0.332 | 1.861 |
| MODIS | 32 (12.03) | < 0.5% | | 0.151 | 0.563 | 3.180 | 0.098 | 0.375 | 2.128 |
| | | | | | | | | | |
| ASTER | 10 (8.29) | < 1K | | 0.165 | 0.776 | 4.139 | 0.077 | 0.363 | 1.966 |
| ASTER | 11 (8.63) | < 1K | | 0.103 | 0.613 | 3.273 | 0.049 | 0.297 | 1.620 |
| ASTER | 12 (9.08) | < 1K | 69 | -0.305 | 0.613 | 3.082 | -0.157 | 0.310 | 1.546 |
| ASTER | 13 (10.66) | < 1K | | -0.252 | 0.464 | 2.344 | -0.152 | 0.278 | 1.387 |
| ASTER | 14 (11.29) | < 1K | | -0.118 | 0.489 | 2.568 | -0.077 | 0.310 | 1.602 |

## IX. SUMMARY AND CONCLUSION

The absolute radiometric calibration accuracy of the ASTER TIR channels and MODIS-Terra MIR and TIR channels was assessed from early 2000 to late 2005 using water skin and bulk temperature data from an automated validation site at Lake Tahoe, CA/NV. The bulk and skin temperature data are acquired every 2–5 min from four permanently moored buoys on the lake. Assessment involved taking the skin temperature at the time of the overpass and predicting the vicarious at-sensor radiance with a radiative transfer model. The vicarious at-sensor radiance was then convolved with the instrument system response function and compared with the radiance measured by ASTER and MODIS-Terra in the MIR and TIR wavelength regions.

TIR data from 69 ASTER and 155 MODIS-Terra scenes were validated at the Lake Tahoe site. Seventy-eight of the MODIS-Terra scenes, which were acquired at night, were also used to validate the MIR data from MODIS-Terra. All the scenes that were validated were acquired when the Terra platform was nearly overhead in order to minimize the effects of view angle on the validations. ASTER data that were acquired with the lake slightly off center (15 dates) were acquired by pointing the instrument no more than $\pm 8.6^\circ$ off nadir.

The percent difference between the predicted and instrument at-sensor radiances for ASTER channels 10–14 was $0.165 \pm 0.776$, $0.103 \pm 0.613$, $-0.305 \pm 0.613$, $-0.252 \pm 0.464$, and $-0.118 \pm 0.489$, respectively. Similarly, the percent difference for MODIS-Terra land-monitoring channels 29, 31, and 32 were $0.082 \pm 0.631$, $0.044 \pm 0.541$, and $0.151 \pm 0.563$; the results for MODIS-Terra MIR channels 20, 22, and 23 were $-1.375 \pm 0.973$, $-1.743 \pm 1.027$, and $-0.898 \pm 0.970$, respectively. These results are summarized in Table I and indicate that the instrument-calibrated radiances of the ASTER and MODIS-Terra TIR channels continue to meet the preflight specification, provided that the ASTER channels are corrected for the additional drift between LTCs. The measured radiances for the MODIS-Terra MIR channel are greater than expected, and the validation data indicate that the MIR channels show greater bias than expected based on the preflight calibration accuracy specification.

If MODIS and ASTER data are to be used as climate date records (CDRs) or Earth system data records (ESDRs), it is essential to demonstrate that the data meet the calibration specification, and the periodic instrument calibration accurately compensates for any change in performance of the instrument with time. Data from Lake Tahoe, CA/NV, or similar data from other sites are essential to validate the accuracy of the ESDRs or CDRs.

## ACKNOWLEDGMENT

Numerous people have contributed to this paper. In particular, the authors would like to thank R. C. Richards and B. Allen (University of California, Davis); R. Alley, A. Abtahi, and F. Palluconi (JPL); and C. Moeller (University of Wisconsin) for providing numerous helpful suggestions.

## REFERENCES

[1] W. L. Barnes, T. S. Pagano, and V. V. Salomonson, "Pre-launch characteristics of the Moderate Resolution Imaging Spectroradiometer (MODIS) on EOS AM1," *IEEE Trans. Geosci. Remote Sens.*, vol. 36, no. 4, pp. 1088–1100, Jul. 1998.

[2] J. A. Barsi, J. R. Schott, F. D. Palluconi, D. L. Helder, S. J. Hook, B. L. Markham, G. Chander, and E. M. O'Donnell, "Landsat TM and ETM+ thermal band calibration," *Can. J. Remote Sens.*, vol. 29, no. 2, pp. 141–153, 2003.

[3] I. J. Barton, P. J. Minnett, K. A. Maillet, C. J. Donlon, S. J. Hook, A. T. Jessup, and T. J. Nightingale, "The Miami2001 infrared radiometer calibration and inter-comparison: Ship comparisons," *J. Atmos. Ocean. Technol.*, vol. 21, no. 2, pp. 268–283, 2004.

[4] A. Berk, L. S. Bernstein, and D. C. Robertson, "MODTRAN: A moderate resolution model for LOWTRAN 7," Geophys. Lab., Bedford, MA, Tech. Rep. GL-TR-89-0122, 1989.
[5] J. J. Butler and R. A. Barnes, "Calibration strategy for the Earth Observing System (EOS)-AM1 platform," *IEEE Trans. Geosci. Remote Sens.*, vol. 36, no. 4, pp. 1056–1061, Jul. 1998.
[6] S. J. Hook and K. Okada, "In-flight wavelength correction of Thermal Infrared Multispectral Scanner (TIMS) data acquired from the ER-2," *IEEE Trans. Geosci. Remote Sens.*, vol. 34, no. 1, pp. 179–188, Jan. 1996.
[7] S. J. Hook, A. J. Prata, R. E. Alley, A. Abtahi, R. C. Richards, S. G. Schladow, and S. Ó. Pálmarsson, "Retrieval of lake bulk and skin temperatures using Along-Track Scanning Radiometer (ATSR-2) data: A case study using Lake Tahoe, California," *J. Atmos. Ocean. Technol.*, vol. 20, no. 4, pp. 534–548, Apr. 2003.
[8] S. J. Hook, G. Chander, J. A. Barsi, R. E. Alley, A. Abtahi, F. D. Palluconi, B. L. Markham, R. C. Richards, S. G. Schladow, and D. L. Helder, "In-flight validation and recovery of water surface temperature with Landsat-5 thermal infrared data using an automated high-altitude lake validation site at Lake Tahoe," *IEEE Trans. Geosci. Remote Sens.*, vol. 42, no. 12, pp. 2767–2776, Dec. 2004.
[9] S. J. Hook, W. B Clodius, L. Balick, R. E. Alley, A. Abtahi, R. C. Richards, and S. G. Schladow, "In-flight validation of mid and thermal infrared data from the Multispectral Thermal Imager (MTI) using an automated high-altitude validation site at Lake Tahoe CA/NV, USA," *IEEE Trans. Geosci. Remote Sens.*, vol. 43, no. 9, pp. 1991–1999, Sep. 2005.
[10] C. C. Moeller, H. E. Revercomb, S. A. Ackerman, W. P. Menzel, and R. O. Knuteson, "Evaluation of MODIS thermal IR band L1B radiances during SAFARI 2000," *J. Geophys. Res.—Atmos.*, vol. 108, no. D13, p. SAF 30-1, 2003.
[11] A. Ono, F. Sakuma, K. Arai, Y. Yamaguchi, H. Fujisada, P. Slater, K. Thome, F. Palluconi, and H. Kieffer, "Preflight and in-flight calibration plan for ASTER," *J. Atmos. Ocean. Technol.*, vol. 13, no. 2, pp. 321–335, Apr. 1996.
[12] C. Prabhakara and G. Dalu, "Remote sensing of surface emissivity at 9 $\mu$m over the globe," *J. Geophys. Res.*, vol. 81, no. C21, pp. 3719–3724, Jul. 1976.
[13] A. J. Prata, "Land surface temperatures derived from AVHRR and ATSR—Part II: Experimental results and validation of AVHRR algorithms," *J. Geophys. Res.*, vol. 99, no. D6, pp. 13 025–13 058, 1994.
[14] J. P. Rice, J. J. Butler, B. C. Johnson, P. J. Minnett, K. A. Maillet, T. J. Nightingale, S. J. Hook, A. Abtahi, C. J. Donlon, and I. J. Barton, "The Miami2001 infrared radiometer calibration and intercomparison—Part I: Laboratory characterization of blackbody targets," *J. Atmos. Ocean. Technol.*, vol. 21, no. 2, pp. 258–267, Feb. 2004.
[15] J. R. Schott and W. J. Volchok, "Thematic mapper thermal infrared calibration," *Photogramm. Eng. Remote Sens.*, vol. 51, no. 9, pp. 1351–1357, 1985.
[16] V. V. Salomonson, W. L. Barnes, P. W. Maymon, H. E. Montgomery, and H. Ostrow, "MODIS: Advanced facility instrument for studies of the Earth as a system," *IEEE Trans. Geosci. Remote Sens.*, vol. 27, no. 2, pp. 145–153, Mar. 1989.
[17] T. E. Steissberg, S. J. Hook, and S. G. Schladow, "Characterizing partial upwellings and surface circulation at Lake Tahoe, CA/NV, USA with thermal infrared images," *Remote Sens. Environ.*, vol. 99, no. 1/2, pp. 2–15, Nov. 2005.
[18] D. C. Tobin, H. E. Revercomb, C. C. Moeller, and T. S. Pagano, "Use of atmospheric infrared sounder high-spectral resolution spectra to assess the calibration of Moderate Resolution Imaging Spectroradiometer on EOS Aqua," *J. Geophys. Res.—Atmos.*, vol. 111, no. D9, D09S05, 2006.
[19] H. Tonooka, F. D. Palluconi, S. J. Hook, and T. Matsunaga, "Vicarious calibration of ASTER thermal infrared bands," *IEEE Trans. Geosci. Remote Sens.*, vol. 43, no. 12, pp. 2733–2746, Dec. 2005.
[20] Y. Yamaguchi, A. B. Kahle, H. Tsu, T. Kawakami, and M. Pniel, "Overview of Advanced Spaceborne Thermal Emission Reflectance Radiometer," *IEEE Trans. Geosci. Remote Sens.*, vol. 36, no. 4, pp. 1062–1071, Jul. 1998.
[21] J. Wang, G. P. Anderson, H. E. Revercomb, and R. O. Knuteson, "Validation of FASCODE3 and MODTRAN3: Comparison of model calculations with ground-based and airborne interferometer observations under clear-sky conditions," *Appl. Opt.*, vol. 35, no. 30, pp. 6028–6040, Oct. 1996.
[22] Z. Wan and Z.-L. Li, "A physics-based algorithm for retrieving land-surface emissivity and temperature from EOS/MODIS data," *IEEE Trans. Geosci. Remote Sens.*, vol. 35, no. 4, pp. 980–996, Jul. 1997.
[23] Z. M. Wan, Y. L. Zhang, Z. L. Li, R. B. Wang, V. V. Salomonson, A. Yves, R. Bosseno, and J. F. Hanocq, "Preliminary estimate of calibration of the Moderate Resolution Imaging spectroradiometer thermal infrared data using Lake Titicaca," *Remote Sens. Environ.*, vol. 80, no. 3, pp. 497–515, 2002.
[24] Z. Wan, Y. Zhang, Q. Zhang, and Z. L. Li, "Quality assessment and validation of the MODIS global land surface temperature," *Int. J. Remote Sens.*, vol. 25, no. 1, pp. 261–274, 2004.
[25] X. Q. Wu and W. L. Smith, "Emissivity of rough sea surface for 8–13 $\mu$m: Modeling and verification," *Appl. Opt.*, vol. 36, no. 12, pp. 2609–2619, Apr. 1997.

**Simon J. Hook** received the B.Sc. and Ph.D. degrees from the University of Durham, Durham, U.K., in 1982 and 1989, respectively, and the M.Sc. degree from the University of Edmonton, Edmonton, AB, Canada, in 1985.

He is currently a Principal Scientist in the NASA Jet Propulsion Laboratory, California Institute of Technology, Pasadena. He has been involved in the validation of several airborne and spaceborne instruments, including the Advanced Spaceborne Thermal Emission and Reflection Radiometer (ASTER), Landsat (5 and ETM+), the Moderate Resolution Imaging Spectroradiometer (MODIS), the MODIS/ASTER Airborne Simulator, the European Along Track Scanning Radiometers (ATSR2 and AATSR), and the U.S. Department of Energy Multispectral Thermal Imager. His research interests include improving our understanding of geologic and hydrodynamic processes.

**R. Greg Vaughan** received the B.S. degree from Virginia Polytechnic Institute and State University, Blacksburg, in 1992, the M.S. degree from the University of Georgia, Athens, Greece, in 1995, and the Ph.D. degree from the University of Nevada, Reno, in 2004, all in geology.

He is currently a Postdoctoral Scholar in the NASA Jet Propulsion Laboratory, California Institute of Technology, Pasadena. He has been involved in the validation of ASTER and MODIS land surface temperature and emissivity data products using *in-situ* ground measurements. His research interests include analysis and modeling of laboratory, field, airborne, and spaceborne remote sensing data for remote volcano monitoring and surface compositional mapping.

**Hideyuki Tonooka** (M'04) received the B.Eng., M.Eng., and D.Eng. degrees from the University of Tokyo, Tokyo, Japan, in 1992, 1994, and 2000, respectively.

Since 1994, he has been a member of the faculty of Ibaraki University, Ibaraki, Japan, where he is currently an Associate Professor in the Center for Information Technology. He is a member of the Project Science Team for the Advanced Spaceborne Thermal Emission and Reflection (ASTER) radiometer, which is part of the National Aeronautics and Space Administration's Earth Observing System. He is also a member of the Thermal Infrared Science Team for the Greenhouse gas Observing SATellite (GOSAT), which is under development by the Japan Aerospace Exploration Agency and the Ministry of the Environment of Japan. His main research interests include thermal infrared remote sensing and data fusion techniques.

**S. Geoffrey Schladow** received the Ph.D. degree from the University of Western Australia, Crawley, in 1986.

He is a Professor of civil and environmental engineering in the Department of Civil and Environmental Engineering, University of California (UC), Davis, and the Director of the UC Davis Tahoe Environmental Research Center. His research interests include mixing and transport processes in aquatic systems, water quality modeling, and the linkages between fluid mechanics and the determinants of water quality and ecological well-being.